Ionics (2006) 12:371–378
DOI 10.1007/s11581-006-0062-y

SHORT COMMUNICATION

Structural, magnetic and electrochemical studies on $LiCo_{0.5}Fe_{0.5}O_2$

D. Kalpana · R. Justin Joseyphus · N. Sivakumar · A. Narayanasamy · M. V. Ananth

Received: 1 November 2006 / Accepted: 9 December 2006 / Published online: 12 January 2007

Abstract $LiCo_{0.5}Fe_{0.5}O_2$ was prepared by sol–gel method. The sample had spinel, cubic and hexagonal phases up to 873 K and a single hexagonal phase above 1,073 K. The magnetic properties were studied at room temperature and at 77 K. The large coercivities observed for the samples annealed at 1,073 and 1,273 K show that these samples do not exhibit a simple antiferromagnetic ordering. From the Mössbauer and magnetization measurements, it is concluded that the hexagonal phase is only an antiferromagnet. The above results clearly demonstrate that the simple aqueous-based sol–gel process developed in this work provides a viable method to synthesize the fine cuboidal particles that display discharge capacity as high as ≈165 mAh/g, which is higher than the value obtained by M. Holzapfel et al. (Holzapfel M, Schreiner R, Ott A, Electrochim Acta 46:1063, 2001) for their samples synthesized by using the ion exchange method. This work suggests that the approaches based on solution chemistry are viable processes for synthesizing good quality electrode material.

Keywords Lithium-ion batteries · Lithium cobalt oxide · $LiCo_{0.5}Fe_{0.5}O_2$ · Mössbauer effect · Triangular antiferromagnetism

D. Kalpana (✉) · M. V. Ananth
Central Electrochemical Research Institute,
Karaikudi 630 006, India
e-mail: dkalps@rediffmail.com

R. J. Joseyphus · N. Sivakumar · A. Narayanasamy
Materials Science Centre, Department of Nuclear Physics,
University of Madras,
Guindy Campus,
Chennai 600 025, India

Introduction

Rechargeable secondary batteries are in great demand as power sources for portable electronic equipments because of their high energy density. In recent years, there has been much interest and effort in developing lithium secondary batteries, as they exhibit lightweight, high voltage and high discharge capacity [1–5]. The cathode material $LiCoO_2$ is receiving much importance for application in commercial rechargeable lithium micro-batteries [6].

The compound $LiCoO_2$, with a layered structure, is an attractive positive electrode material for lithium-ion batteries because of its relatively larger discharge capacity and lower cost. It has a hexagonal structure, which is easy to prepare with the ideal layered configuration (c/a ratio= 4.99) [7]. It also exists in trigonal symmetry [8, 9].

$LiFeO_2$ has several polymorphs such as cubic disordered rock salt structure α-$LiFeO_2$, monoclinic ordered rock salt type β-$LiFeO_2$, rhombohedral γ-$LiFeO_2$ and orthorhombic $LiFeO_2$ [10, 11]. Of these polymorphs, only orthorhombic corrugated layered structure [12–14] and an orthorhombic Goethite-type structure show good electrochemical activity [15]. In the case of layered $LiNiO_2$, the electrochemical activity and also the electrochemical stability could be enhanced by substituting Co partially for Ni [16–20].

These lithium transition metal oxides, depending on the preparation techniques, vary in discharge capacities. In particular, the conventional thermally driven solid state reactions have a tendency to yield coarse-grained agglomerated powders with compositional inhomogeneities [21, 22], and such coarse-grained materials show poor battery activity. To overcome these deficiencies, interest has been focused now on low-temperature synthetic routes such as co-precipitation, sol–gel, alkoxide hydrolysis and a citrate

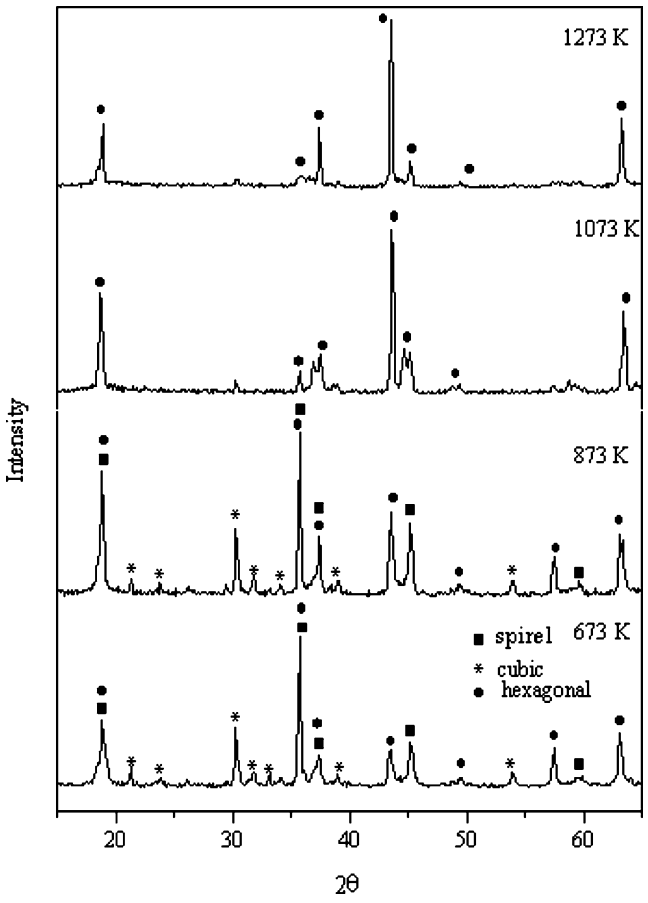

Fig. 1 The XRD spectra for the $LiCO_{05}Fe_{05}O_2$ sample appealed at different temperatures

route that results in fine grains [23–27]. The choice of the synthetic route and the starting materials greatly affects the energy and power densities [28–30]. To investigate whether the partial substitution of Co in $LiFeO_2$ will enhance the electrochemical activity of $LiFeO_2$, the system $LiCo_{0.5}Fe_{0.5}O_2$ has been synthesized by sol–gel method, and the suitable conditions such as heat-treating temperature and duration of the synthesis are investigated for enhancing the electrochemical activity. The synthesized materials were examined in terms of their crystal structure and morphology. The physical properties such as magnetization and hyperfine interactions were studied. The preparation conditions and structural details are correlated with the electrochemical properties.

Table 1 Structural parameters of the $LiCo_{0.5}Fe_{0.5}O_2$ sample annealed at various temperatures

Annealing temperature of the sample (K)	Lattice parameters (Å)		Cell volume (Å^3)	Crystal phase
	a	c		
673	7.99	14.35	510.08	Spinel
	2.87		102.37	Hexagonal
	4.15		71.47	Cubic
873	7.97	14.30	506.26	Spinel
	2.88		102.72	Hexagonal
	4.15		71.47	Cubic
1,073	2.95	14.16	106.72	Hexagonal
1,273	2.94	14.40	107.79	Hexagonal

Experimental procedure

Materials synthesis and characterization

Sol–gel method was used for synthesizing $LiCo_{0.5}Fe_{0.5}O_2$ powders. Equimolar amounts of lithium acetate, cobalt acetate and α-Fe_2O_3 were mixed with distilled water. Methanol with a volume of 500 ml was used as a solvent to dissolve the stoichiometric amounts of lithium and cobalt precursors. The acetates were mixed with distilled water, and it was stirred well with the solvent. Dark purple colour suspensions of colloidal particles were obtained. The gel was then dried to yield organic polymer foam. This dried xerogel product thus obtained was then ground into a fine powder.

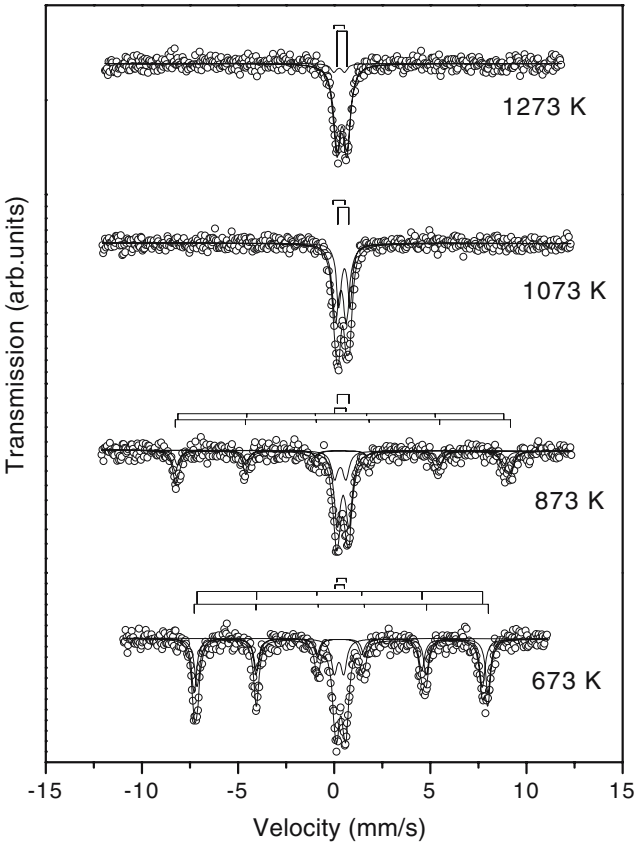

Fig. 2 The Mössbauer spectra recorded at 298 K of the samples annealed at various temperatures

Table 2 Mössbauer parameters of $LiCo_{0.5}Fe_{0.5}O_2$ annealed at various temperatures

Annealing temperature (K)	Mössbauer parameters					Phases identified
	H_{hf} (kOe) ± 2.0	CS (mm/s) ± 0.01	QS (mm/s) ± 0.02	WV (mm/s) ± 0.01	Relative intensity (%)	
673	473	0.47	−0.01	0.31	32.9	Spinel
	459	0.38	−0.03	0.34	32.0	Spinel
	–	0.49	0.49	0.36	23.4	Hexagonal
	–	0.36	0.49	0.37	11.7	Cubic
873	468	0.50	0.01	0.33	24.2	Spinel
	455	0.41	0.01	0.35	17.7	Spinel
	–	0. 52	0.52	0.36	42.5	Hexagonal
	–	0. 39	0.51	0.34	15.6	Cubic
1,073	–	0.52	0.49	0.34	90.5	Hexagonal
	–	0.33	0.52	0.33	9.5	Cubic
1,273	–	0.52	0.52	0.43	91.7	Hexagonal
	–	0.37	0.56	0.37	8.3	Cubic

H_{hf} Hyperfine magnetic field, *CS* centre shift, *QS* quadrupole splitting, *WV* line width

Fine powders were produced by calcining the precursors in air at various temperatures for a few hours. The powders were then heat-treated in a furnace at four different temperatures at 673, 873, 1,073 and 1,273 K for 6 h.

The heat-treated product was ground, and the fine powders were then analyzed for their structure and magnetic properties using X-ray diffractometer (Stoe, Germany) with CuKα radiation, Vibrating Sample Magnetometer (EG & G Parc, Model 4500) with a maximum field of 7 kOe and a constant acceleration Mössbauer spectrometer (Weissel, Germany, Model No. MDU-1200) with ^{57}Co (Rh) Mössbauer source kept at room temperature. The Mössbauer spectra were fitted with the least-squares method developed by Bent et al. [31]. The study of the morphology of the heat-treated powders was carried out with a JEOL-JSM-840A-Scanning Electron Microscope. The charge–discharge characteristics of the cells were carried out in an argon-filled glove box.

Cell assembly

One of the characteristic features of lithium-ion batteries is the flexibility in cell design. One can choose a suitable voltage together with a cell capacity by selecting insertion materials for the positive and negative electrodes. The experimental cell with these electrodes was used to evaluate the electrochemical performance of these cathodes. The cathode mixture was prepared by adding $LiCo_{0.5}$ $Fe_{0.5}O_2$ powder (40 mg) and 8 mg of acetylene black powder (to provide the required electrical conductivity) with polytetra-fluoro-ethylene as binder. Lithium metal was used as an anode. The electrolyte used was a 1-M $LiPF_6$ solution in 66 wt% ethylene carbonate and 33 wt% propylene carbonate that was soaked onto a separator. The entire cell was assembled in an argon-filled glove box. The cells were tested using a constant current of 0.25 mA in the voltage range of 4.2 to 2.9 V.

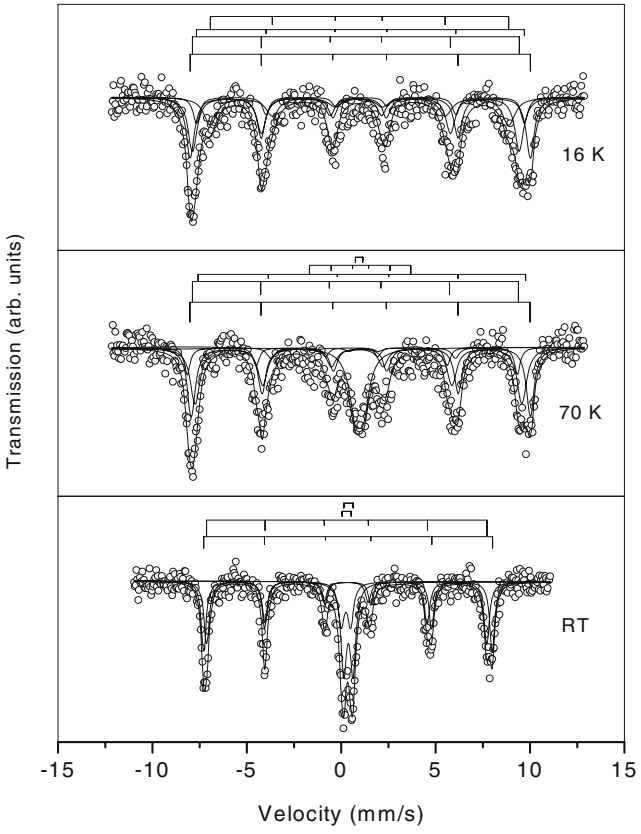

Fig. 3 The Mössbauer spectra at 298, 70 and 16 K for the sample annealed at 673 K

Table 3 Mössbauer parameters of the 673-K annealed $LiCo_{0.5}Fe_{0.5}O_2$ sample measured at various temperatures

Temperature (K)	Mössbauer parameters					Phases
	H_{hf} (kOe) ±2.0	CS (mm/s) ±0.01	QS mm/s) ±0.02	WV (mm/s) ±0.01	Relative intensity (%)	
298	473	0.47	−0.01	0.31	32.9	Spinel B site
	459	0.38	−0.03	0.34	32.0	Spinel A site
	–	0.36	0.49	0.37	11.7	Cubic
	–	0.49	0.49	0.36	23.4	Hexagonal
70	539	0.56	0.02	0.64	32.9	Spinel B site
	517	0.33	0.02	0.62	32.0	Spinel A site
	520	0.69	0.05	0.45	10.4	Hexagonal
	161	0.59	0.02	0.73	13.0	Hexagonal
	–	0.52	0.37	0.69	11.7	Cubic
16	539	0.59	0.03	0.53	32.9	Spinel B site
	518	0.33	0.00	0.55	32.0	Spinel A site
	520	0.59	0.03	0.54	23.4	Hexagonal
	473	0.50	0.00	0.44	11.7	Cubic

H_{hf} Hyperfine magnetic field, *CS* centre shift, *QS* quadrupole splitting, *WV* line width

Results and discussions

X-ray analysis

The X-ray diffraction (XRD) patterns for the materials heat-treated at various temperatures for 6 h in air are given in Fig. 1. The dominant peaks of the sample annealed at 673 K could be indexed to the lithiated-spinel $Li_2[Co_2]O_4$ structure [32] along with the cubic and hexagonal phases. It is noted that the spinel phase disappears on annealing the sample at 1,073 K. A hexagonal phase was obtained at 1,073 K according to the XRD results shown in Fig. 1 with small traces of cubic phase as indicated by the additional reflections at $2\theta=30.3°$ and $2\theta=39.3°$. In this layered structure, alternate layers of Li and M occupy the octahedral sites of a cubic close packing arrangement of oxygen ions, making up a rhombohedral structure with Li in 3a, M in 3b and O in 6c sites. It is assumed that there may be a partial disorder of M^{3+} in the 3a sites, which implies a partial occupation of the 3b positions by lithium [33]. The sample has spinel, cubic and hexagonal phases up to 873 K, and almost a single hexagonal phase is formed above 1,073 K, which is favourable to the lithium ion diffusion through the path of the oxide. The structural parameters obtained from the analysis of the X-ray data are given in Table 1.

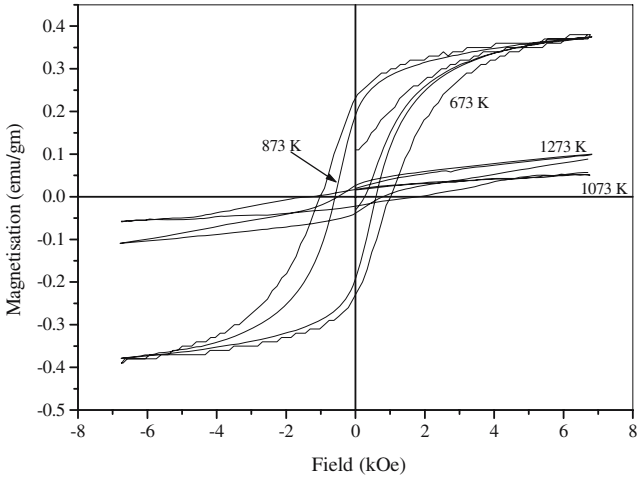

Fig. 4 The magnetization at 77 K of $LiCo_{0.5}Fe_{0.5}O_2$ annealed at various temperatures

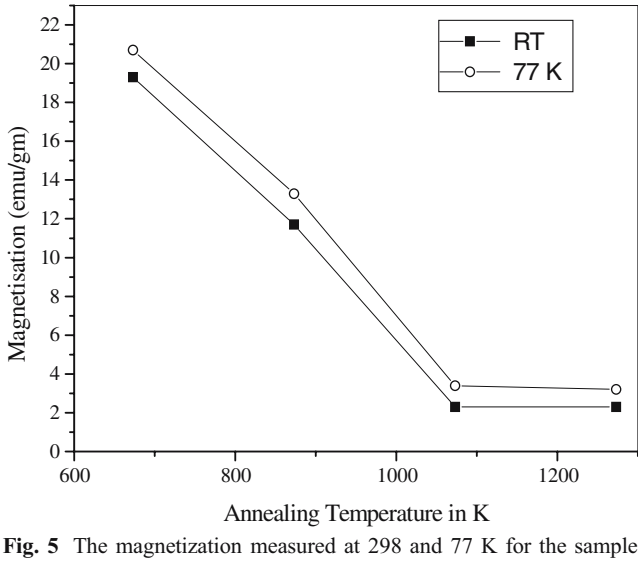

Fig. 5 The magnetization measured at 298 and 77 K for the sample annealed at different temperatures. The *continuous lines* are guide to the eyes

Table 4 The saturation magnetization, coercivity and remanence ratio of $LiCo_{0.5}Fe_{0.5}O_2$ annealed at various temperatures

Annealing temperature of the sample (K)	M_s (emu/gm)		H_c (Oe)		M_r/M_s	
	298 K	77 K	298K	77 K	298 K	77 K
673	19.3	20.7	285	1,022	0.36	0.59
873	11.7	13.3	209	591	0.31	0.50
1,073	2.3	3.4	820	1,572	0.42	0.34
1,273	2.3	3.2	685	643	0.37	0.30

M_s Saturation magnetization, H_c coercivity, M_r/M_s remanence ratio

Mössbauer analysis

The Mössbauer spectra recorded at 298 K of the samples annealed at various temperatures are shown in Fig. 2. The Mössbauer spectrum of the sample annealed at 673 K was fitted with two sextets and two doublets. The two sextets correspond to the magnetically ordered phase of the spinel structure. The relative intensity of the sextets decreases on annealing the samples at higher temperatures. The relative intensities were treated as free parameters, with least squares fitting the data. The sextets arise from the tetrahedral (A) and octahedral (B) ^{57}Fe sites of the spinel phase with internal magnetic fields of 459 and 473 kOe, respectively, at room temperature (Table 2). The corresponding chemical shifts (CS) are 0.38 and 0.47 mm/s (relative to metallic Fe at 298 K), respectively. The sextet with a more positive chemical shift and internal magnetic field of 473 kOe is assigned to the ^{57}Fe atoms in the octahedral site and the other sextet with a smaller value for chemical shift to the ^{57}Fe atoms in the tetrahedral site. The two doublets arise from the ^{57}Fe atoms in the hexagonal and cubic phases. For the samples annealed at 1,073 and 1,273 K, the sextets disappear, as the spinel phase is not present as is evident from the XRD. The Mössbauer spectra have been fitted with two doublets corresponding to the hexagonal and cubic phases. The relative intensity of the doublet from the cubic phase decreases with annealing temperature in accordance with the XRD results. The values of the CS and the quadrupole splitting are characteristic of the ferric ion.

To confirm whether the cubic and hexagonal phases are magnetic or non-magnetic, the low-temperature Mössbauer measurements were carried out for the sample annealed at 673 K. Figure 3 shows the Mössbauer spectra at 298, 70 and 16 K for the sample annealed at 673 K. At 16 K, the Mössbauer spectrum is fitted with four sextets; two sextets arise from the tetrahedral and octahedral Fe sites of the spinel phase, the other two arise from the cubic and hexagonal phases, and the Mössbauer parameters obtained from the fitting are presented in Table 3. At 70 K, the quadrupole split doublet is assigned to the Fe atoms in the cubic phase as guided by the isomer shift and the intensity of this doublet obtained at 298 and at 70 K. This shows that the magnetic ordering temperature of the cubic phase is smaller than that of the hexagonal phase. The sextet at 70 K with an internal magnetic field of 520 kOe is attributed to the Fe atoms in the hexagonal phase. The addition of another sextet with a smaller internal magnetic field of 161 kOe was necessitated for a satisfactory fitting. Judging from the relative intensity of the Mössbauer spectrum of the

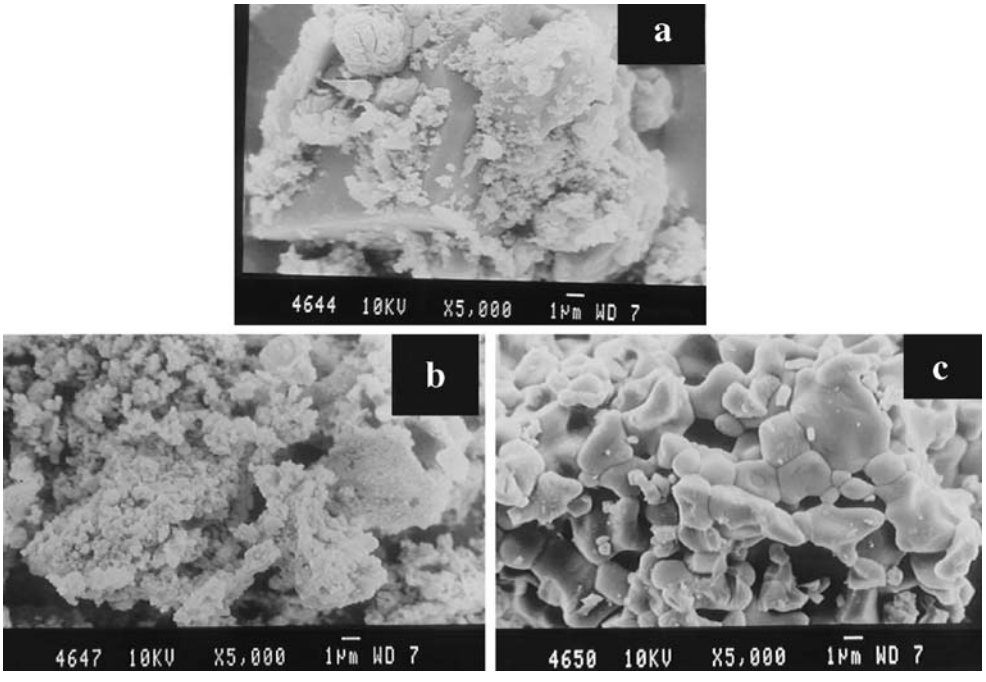

Fig. 6 The SEM of $LiCo_{0.5}Fe_{0.5}O_2$ **a** as-prepared and sample annealed at **b** 873 K and **c** 1,273 K

hexagonal phase both at 298 and at 70 K, one can easily conclude that this low-field sextet also originates from the hexagonal phase. If the magnetic ordering temperature of the hexagonal phase is very close to 70 K, there is a possibility for the existence of such low-field components. However, at temperatures much below the ordering temperature, the low-field components should saturate as obtained in the present study, where we have observed that the internal magnetic field of the hexagonal phase saturates to 520 kOe at 16 K.

Magnetization measurements

The M–H curves recorded at room temperature are given in Fig. 4 for the samples annealed at 673, 873, 1,073 and 1,273 K, and Fig. 5 shows the variation of M_s at 298 and 77 K as a function of annealing temperature. The values of the spontaneous magnetization M_s, the remanence ratio M_r/M_s, and the coercivity are given in Table 4. As seen from Table 4, the value of M_s is higher for the samples annealed at 673 and 873 K; of course, M_s is lower for the sample annealed at 873 K compared to that of the other sample. On annealing at 1,073 and 1,273 K, M_s reduces to a negligible value of 2.3 emu/g at 298 K. These values of M_s can be accounted for on the basis of the crystalline phases present after annealing at various temperatures. As seen from the XRD measurements, the spinel phase is present for the samples annealed at 673 and 873 K, with the volume fraction of this phase being smaller for the sample annealed at 873 K. The spinel phase shows magnetic ordering at 298 K as is evident from Mössbauer measurements. Therefore, the ferrimagnetic ordering of the spinel phase gives rise to appreciable values for M_s on annealing at 673 K, which decreases on annealing at 873 K due to the decrease in the fractional volume of the spinel phase. On annealing at 1,073 and 1,273 K, the spinel phase disappears as seen from XRD and Mössbauer measurements. Only hexagonal and cubic phases are present on annealing at these two higher temperatures. These two phases are in their paramagnetic state at 298 K as shown by a doublet in the Mössbauer spectrum in Fig. 2. At 77 K, the hexagonal phase is magnetically ordered, and the cubic phase is still paramagnetic as revealed by the Mössbauer spectrum given in Fig. 3. The values of M_s at 77 K for the samples annealed at 1,073 and 1,273 K are 3.4 and 3.2 emu/g, which are still low only. From the Mössbauer and magnetization measurements, we, therefore, conclude that the hexagonal phase is not ferromagnetically nor ferrimagnetically ordered; it should be only an antiferromagnet, may be a triangular antiferromagnet as reported by K. Hirakawa et al. [34].

The remanence ratio (M_r/M_s) at 298 K for all the annealed samples shows a value less than 0.5, which is a characteristic feature of the non-interacting isolated particles. The large coercivities observed for the samples annealed at 1,073 and 1,273 K also show that these samples are not exhibiting a simple antiferromagnetic ordering.

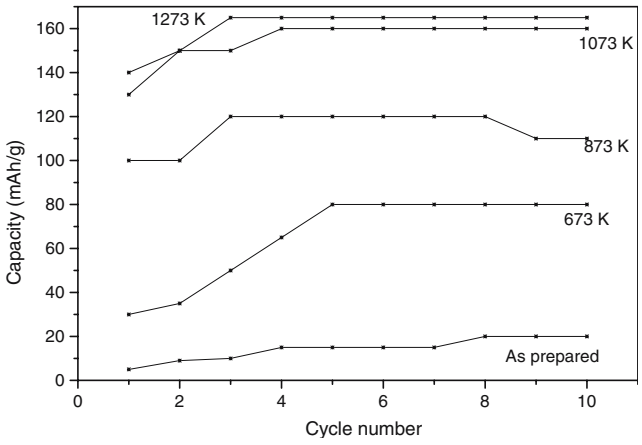

Fig. 7 The discharge characteristics of $LiCo_{0.5}Fe_{0.5}O_2$ sample annealed at different temperatures

Morphology of the heat-treated $LiCo_{0.5}Fe_{0.5}O_2$ powders

The morphology of all the heat-treated powders derived from the aqueous solution of the acetates was obtained using scanning electron microscopy (SEM). Figure 6 shows the SEM photographs of the powders of the as-prepared sample and for the samples annealed at 873 and 1,273 K, respectively, for 6 h. The SEM micrograph of the as-prepared sample reveals clusters of particles ranging in size from one to several microns. On heat treatment to 873 K, it can be seen that the particles have grown in size as expected and have undergone necking to form agglomerates of several microns. It can also be seen that the particles have begun to attain a definite cuboidal shape.

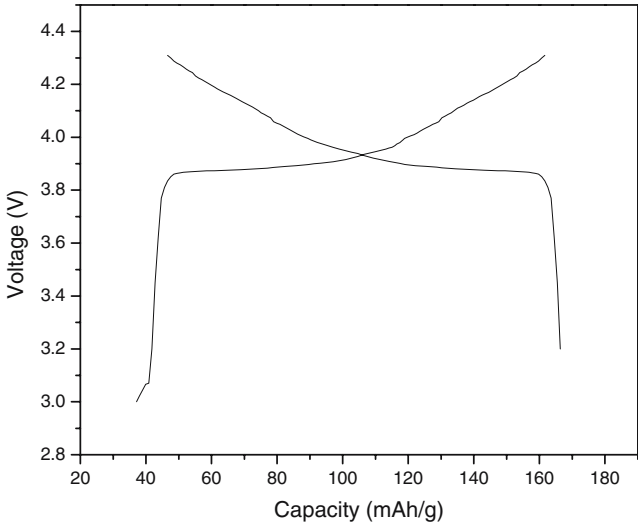

Fig. 8 Charge–discharge profile of $LiCo_{0.5}Fe_{0.5}O_2$ annealed at 1,273 K

Subsequent heat treatment of the precursor to 1,273 K results in further growth of the particles, and it can be seen that the microstructure of the powders is now comprised of large clusters. An important aspect to note is that the heat treatment at 1,273 K has resulted in more faceting, and the particles exhibit a definite regular cuboidal shape as opposed to the heat treatments conducted at 873 K and for the as-prepared samples.

Analysis of electrochemical properties

The electrochemical properties of $LiCo_{0.5}Fe_{0.5}O_2$ annealed at various temperatures were characterized by cycling tests (10 cycles). Figure 7 shows the discharge characteristics of the as-prepared $LiCo_{0.5}Fe_{0.5}O_2$ and annealed at 673, 873, 1,073 and 1,273 K. The sample annealed at 673 K has a relatively small initial capacity and poor rechargeability due to the presence of spinel phase. The Co in the octahedral sites of the spinel may be blocking the diffusion of Li^+ ions, and hence the electrochemical activity is poor for the samples annealed at 673 and 873 K. Similar observations have also been reported by M. Holzapfel et al. [35]. There is a remarkable increase in the discharge capacity for the sample annealed at 1,273 K, as it has almost a single hexagonal phase and is free from the spinel phase. Figure 8 shows the charge–discharge profile of $LiCo_{0.5}Fe_{0.5}O_2$ powder annealed at 1,273 K. Rechargeability is improved as the annealing temperature increases. This is due to the improved crystallinity from multiphase transition to single phase transition. It is clear, therefore, that the powders obtained at 1,273 K employing the sol–gel process certainly perform very well, and the efficiencies are within the acceptable test limits expected for $LiCoO_2$ [36, 37].

Based on the present results, it appears that well-defined fine cuboidal particles do provide good electrochemical characteristics. These fine particles could perhaps provide easier diffusion paths for the de-intercalation of lithium ions, which is the cause for the high capacity during the first charge for the sample annealed at 1,273 K. A change in the crystal structure of the $LiCo_{0.5}Fe_{0.5}O_2$ phase could induce expansion and contraction of the particles, thereby causing fragmentation and separation of the particles in contact. This could also lead to a drop in the capacity during cycling of the sample annealed at 673 K as is displayed in Fig. 7.

The above results clearly demonstrate that the simple aqueous-based sol–gel process developed in this work provides a viable method to synthesize the fine cuboidal particles that display discharge capacity as high as ≈165 mAh/g, which is higher than the value obtained by M. Holzapfel et al. [38] for their samples synthesized by using the ion exchange method. This work suggests that the approaches based on solution chemistry are viable processes for synthesizing good quality electrode material.

Conclusion

An aqueous solution-based process has been developed for synthesizing $LiCo_{0.5}Fe_{0.5}O_2$ powder. The as-prepared xerogels obtained by drying the aqueous solutions indicate the formation of single phase upon heat treatment at 1,273 K for 6 h. The oxide begins to evolve at a temperature as low as 673 K along with the spinel phase. Further heat treatments to 873 and 1,073 K for 6 h result in almost complete elimination of the spinel phase and lead to the formation of the desired phase of $LiCo_{0.5}Fe_{0.5}O_2$. The microstructure of the powders synthesized at low temperature consists of irregularly shaped cluster of particles. The particle morphology begins to evolve upon heat treatment beyond 673 K. The heat treatment at 1,273 K results in well-faceted cuboidal particles that lead to good electrochemical activity. Structure analysis using X-ray powder diffraction has shown that the samples are of good crystallinity, and this is reflected in electrochemical properties. The maximum discharge capacity was obtained for the sample annealed at 1,273 K having single hexagonal phase. From the Mössbauer and magnetization measurements, it is concluded that the hexagonal phase is only an antiferromagnet.

References

1. Ohzuku T, Ueda A (1994) Solid State Ion 69:201
2. Dahn JR, Sleigh AK, Zhong Q, von Sacken U (1993) In: Pistoia G (ed) Lithium batteries. Elsevier, Amsterdam
3. Yoshiyasu S et al (1997) Thermal studies on lithium-ion battery. J Power Sources 68:451
4. Ohzuku T, Ueda A (1994) J Electrochem Soc 141:2972
5. Reimers JN, Dahn JR (1992) J Electrochem Soc 139:2091
6. Abe H, Zaghib K, Tatsumi K, Higuchi S (1995) J Power Sources 54:236
7. Sheur SP, Yao CY, Chen JM, Chio YC (1997) J Power Sources 68:533
8. Yao CY, Kao TH, Cheng CH, Chen JM, Hurng WM (1995) J Power Sources 54:491
9. Dreher J, Hass B, Hambitzer G (1993) J Power Sources 43–44:533
10. Famery R, Bassoul P, Queyroux F (1985) J Solid State Chem 57:178
11. Famery R, Bassoul P, Queyroux F (1986) J Solid State Chem 61:293
12. Kanno R, Shirane T, Inaba Y, Kawamoto Y (1997) J Power Sources 68:145
13. Kanno R, Shirane T, Inaba Y, Kawamoto Y, Takeda Y, Takano M, Ohashi M, Yamaguchi Y (1996) J Electrochem Soc 143:2435
14. Sakurai Y, Arai H, Okada S, Yamaki J (1997) J Power Sources 68:711
15. Rougier A, Saadoune I, Gravereau P, Willmann P, Delmas C (1996) Solid State Ion 90:83
16. Saadoune I, Delmas C (1998) J Solid State Chem 136:8
17. Zhecheva E, Stoyanova R (1993) J Solid State Chem 66:143
18. Fujita Y, Amine K, Mairuta J, Yasuda H (1997) J Power Sources 68:126

19. Tabuchim M, Ado K, Kobayashi H, Sakaeba H, Kageyama H, Masquelier C, Yonemura M, Hiranao A, Kanno R (1999) J Mater Chem 9:199
20. Mizushima K, Jones PC, Wiseman PJ, Goodenough JB (1980) Mater Res Bull 15:783
21. Delmas C, Braconnier J-J (1982) Paul Mater Res Bull 17:117
22. Sato H, Takahashi D, Nishina T, Uchida I (1997) J Power Sources 68:540
23. Banov B, Bourilkov J, Mladenov M (1995) J Power Sources 54:208
24. Abraham KM, Pasquarello DM, Willstaedt EM (1998) J Electrochem Soc 45:198
25. Sekai K, Azuma H, Omaru A, Fujita S, Imoto H, Endo T, Yamaura K, Nishi Y (1993) J Power Sources 43–44:241
26. Rabou LPLM, Roskam A (1995) J Power Sources 54:316
27. Yang CY, Cheng CH, Ho SM, Chen JC, Hurng WM (1997) J Power Sources 68:440
28. Nohma T, Kurokawai H, Uehara M, Takahashi M, Nishio K, Saito T (1995) J Power Sources 54:522
29. Alcantara R, Lavela P, Tirado JL (1998) J Electrochem Soc 145:3
30. Yozami R, Lebrun N, Bonneau M, Molteni M (1995) J Power Sources 54:389
31. Bent MF, Persson P, Agresti DG (1968) Comput Phys Commun 1:67
32. Shao-Horn Y, Hackney SA, Hahaian AJ, Thackery MM (2002) J Solid State Chem 168:60
33. Chappel E, Holzapfel M, Chouteau G, Ott A (2000) J Solid State Chem 154:451
34. Hirakawa K, Kadowaki H (1986) Physica 136B:335
35. Holzapfel M, Haak C, Ott A (2001) J Solid State Chem 156:470
36. Nagura T (1990) In: Proceedings of the fifth international seminar on lithium battery technology and applications, Deerfield Beach, FL, March 5–7
37. Ozawa K (1994) Solid State Ion 69:212
38. Holzapfel M, Schreiner R, Ott A (2001) Electrochim Acta 46:1063